International Journal of Minerals, Metallurgy and Materials
Volume 20, Number 2, February 2013, Page 166
DOI: 10.1007/s12613-013-0709-4

Effect of Co substitution on the structural, electrical, and magnetic properties of $Bi_{0.9}La_{0.1}FeO_3$ by sol-gel synthesis

Ghulam Ali[1)], *Saadat A. Siddiqi*[1,2)], *Shahid M. Ramay*[3)], *Shahid Atiq*[1)], *and Murtaza Saleem*[1)]

1) Centre of Excellence in Solid State Physics, University of the Punjab, Lahore 54590, Pakistan

2) Interdisciplinary Research Centre in Biomedical Materials, COMSATS Institute of Information Technology, Lahore 54590, Pakistan

3) Chemical Engineering Department, College of Engineering, King Saud University, Riyadh 11421, Saudi Arabia

(Received: 5 January 2012; revised: 10 March 2012; accepted: 11 April 2012)

Abstract: Cobalt (Co)-doped $Bi_{0.9}La_{0.1}FeO_3$ multiferroics were synthesized by a sol-gel method based on the auto-combustion technique. As-synthesized powder was examined using various characterization techniques to explore the effect of Co substitution on the properties of $Bi_{0.9}La_{0.1}FeO_3$. X-ray diffraction reveals that Co-doped $Bi_{0.9}La_{0.1}FeO_3$ preserves the perovskite-type rhombohedral structure of $BiFeO_3$, and the composition without Co preserves the original structure of the phase; however, a second-phase $Bi_2Fe_4O_9$ has been identified in all other compositions. Surface morphological studies were performed by scanning electron microscopy. Temperature-dependent resistivity of the samples reveals the characteristic insulating behavior of the multiferroic material. The resistivity is found to decrease with the increase both in temperature and Co content. Room temperature frequency-dependent dielectric measurements were also reported. Magnetic measurements show the enhancement in magnetization with the increase in Co content.

Keywords: multiferroics; cobalt; doping; microstructure; electric properties; magnetic properties; sol-gel process

1. Introduction

Multiferroic materials usually contain at least two of the ferroic order parameters (ferromagnetic, ferroelectric, and ferroelastic) in a single phase. Due to the unique physical properties from this coexistence of several order parameters, multiferroics have attracted extraordinary scientific interest [1-2]. The magnetoelectric (ME) coupling is the key feature for multiferroic devices. If the coupling between magnetization (M) and electric polarization (P) is sufficiently strong, M can be controlled by electric field, and vice versa. This mechanism is very useful for the information storage in memory devices with four logic states ($\pm M$, $\pm P$) [3].

For the material, an effective control of magnetic behavior in connection with electric field widens the applications of spin electronics. Lim *et al.* [4] theoretically predicted the ME effect for the first time, and then Shtrikman *et al.* [5] confirmed it in experiment. Afterwards, a number of magnetic materials have been developed to display this effect. However, the achieved value of ME effect was too small to satisfy the device applications [6-7]. Single-phase multiferroic properties have been, so far, recognized only in perovskite oxide materials. These properties are usually attained by the stereochemical action of lone pair on A-site (cations in A-site offer the ferroelectricity) and holding magnetism on B-site (the smaller cations). This situation in $BiFeO_3$ (BFO) is most extensively studied for single-phase multiferroics (antiferromagnetic and ferroelectric) [8]. At room temperature, BFO has two order parameters: (i) a high Curie temperature ferroelectric ordering; (ii) a magnetic transition, G-type canted antiferromagnetic ordering [9-11].

For the basic properties of ferroelectromagnetic materials, multiferroics are the potential candidates for modern device applications. For example, these materials play a significant role in sensors and spintronic devices [12-13]. However, there are still some restrictions for application

Corresponding author: Shahid Atiq E-mail: shahidatiqpasrur@yahoo.com

due to small remnant polarization, high leakage currents, and spiral antiferromagnetic spin arrangements in BFO-based polycrystalline bulk materials. Many researches have been carried out on BFO to modify its ferroelectric and ferromagnetic properties, such as the epitaxial constraint, high magnetic fields, and chemical substitution. In epitaxial BFO thin films, Singh *et al.* [14] reported an enhanced coercive field and remnant polarization. In rare-earth doped BFO samples, the improvement in magnetization has also been reported where a strong involvement in net magnetization takes place due to the magnetic moments of rare earth ions. It is also indicated that the ferromagnetic property in BFO enhanced with the doping of Mn and Sr is related to the suppression of spiral spin structure [13]; and it is quite essential to achieve the multiferroic properties and enhance them with the doping of some other materials. Cobalt (Co) has strong ferromagnetic behavior and is well known as the potential research candidate due to the strong magnetic interactions. Therefore, the present study aimed to investigate the effect of Co on the structural, electrical, and magnetic behavior of $Bi_{0.9}La_{0.1}FeO_3$.

2. Experimental

BFO was prepared by a sol-gel auto-combustion technique with glycine as a fuel agent. Metal nitrates and glycine (as a precursor) were used to prepare the aqueous solution with the molar ratios of $4BiNO_3(OH)_2{\cdot}BiO(OH)$:$La(NO_3)_3{\cdot}6H_2O$:$Fe(NO_3)_3{\cdot}9H_2O$:glycine as 0.9:0.1:1:2. Stoichiometric proportions of the metal nitrate were dissolved in 75 mL distilled water followed by the addition of stoichiometric glycine. The blend was placed on a hot plate at 120-130°C along with continuous stirring using a magnetic capsule until it became a dark viscous gel. The auto-ignition of the dried gel took place with continuous heating and a large quantity of gases was evolved. The entire procedure took about 90 min, but the time between the actual ignition and the end of reaction was less than 30 s. After the combustion was over, it was further heated for 30 min to complete the combustion of material. As-synthesized powder was grinded and then pelletized using Apex hydraulic press. The pellets were sintered in air at 300°C for 2 h in a muffle furnace (Ogawa Seiki Co., Japan). X-ray diffraction (XRD) patterns of samples were taken using MPD X'PERT PRO of PANalytical Diffractometer under the identical operating conditions. All the patterns were obtained at room temperature using Cu K_α ($\lambda = 15.4178$ nm) radiation to identify the crystal structure and characterize unknown phases. Morphological studies were performed using an S-3400N HITACHI EMAX scanning electron microscope (SEM). Resistivity and dielectric measurements were obtained to explore the electric behavior of samples. Magnetic measurements were carried out by a Lakeshore-7404 vibrating sample magnetometer (VSM).

3. Results and discussion

3.1. XRD analysis

The XRD patterns of compositions are shown in Fig. 1. The analysis indicates the formation of rhombohedral perovskite-like BFO structure. There is no impurity or second phase detected in the composition without Co. However, the diffraction peak marked with an asterisk indicates the formation of an impurity phase ($Bi_2Fe_4O_9$) together with the major BFO phase. This phase has been previously reported during the synthesis of BFO [17-20], and even by a longer calcination time, it can not be removed. It is also clear from the XRD patterns that the peaks are shifted to the lower angles with Co doping due to the larger ionic radius of Co (88 pm), which are larger than that of Fe (78 pm). The overall breadth of characteristic diffraction peaks obtained from the XRD patterns is an indirect sign of change in the crystallite size of all samples. The crystallite size (nm) has been predicted from the X-ray peak broadening; the most intense diffraction peak (110) for all the samples is considered, by means of the Scherrer formula [21] as the following equation.

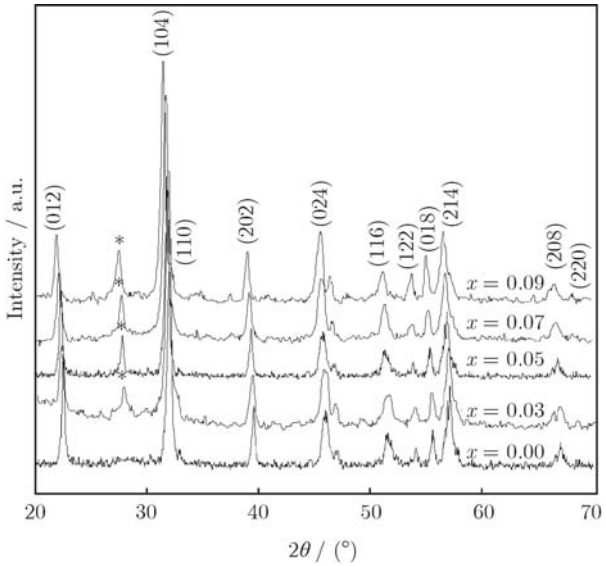

Fig. 1. XRD patterns of $Bi_{0.9}La_{0.1}Fe_{1-x}Co_xO_3$. The peak of the impurity phase ($Bi_2Fe_4O_9$) is marked with an asterisk.

$$\text{Crystallite size} = \frac{0.94\lambda}{B\cos\theta} \tag{1}$$

where θ is the Bragg's angle, B the full-width at half-maximum (FWHM) in radians, and λ the wavelength (λ = 15.4 nm) of Cu K_α radiation used to obtain the XRD patterns. The crystallite size is directly associated with

the ionic radii and lattice parameters. Hence, the change in lattice parameters is correlated with the change in crystallite size. The crystallite size was found in the range of 17-19 nm for all the samples. This small change could be attributed to the small difference in ionic radii of dopant and substituent. The variation of crystallite size with Co doping content is represented in Fig. 2.

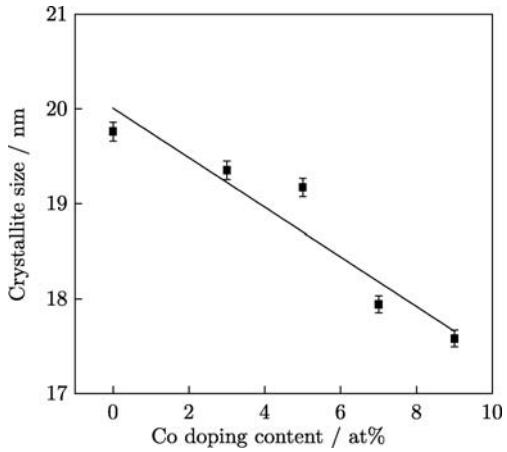

Fig. 2. Crystallite size vs. Co doping content in $Bi_{0.9}La_{0.1}Fe_{1-x}Co_xO_3$.

3.2. SEM analysis

The micrographs of all the samples are shown in Fig. 3. As can be seen in all the micrographs, two kinds of grains are more common: the one bonded together to make larger grains with the well-defined crystalline shape and the others with very small-sized equiaxed grains scattered on the surface at various places. The grain size of these two kinds of grains is estimated as 0.5-4 μm. Some fine grain boundaries with few pores may also be witnessed. In Fig. 3(e), there are large numbers of small grains spread on surface. The estimated grain size of these small equiaxed grains at magnification is less than 0.5 μm. Moreover, some cracks are also found in all micrographs.

3.3. Electrical resistivity

The electrical resistivity of $Bi_{0.9}La_{0.1}FeO_3$ is expected to reduce by the substitution of a small amount of Co at Fe site. The temperature-dependent DC electrical resistivity evaluated for all the samples are shown in Fig. 4. The undoped sample exhibits a maximum value of resistivity of 8.40 GΩ·cm at 160°C, which decreases gradually with the increase in temperature with the value of 1.11 MΩ·cm at 350°C. It is observed that the values of resistivity decrease with the increment in Co content and becomes 0.16 GΩ·cm at 160°C for $x = 0.09$ in $Bi_{0.9}La_{0.1}Fe_{1-x}Co_xO_3$. The improvement in crystallinity due to Co doping, as confirmed by the XRD analysis, might be the reason for a decrease in resistivity with the increase in Co content. The overall trend observed in all the samples was that the value of DC electrical resistivity decreased with the increase of temperature.

3.4. Dielectric measurements

The electronic exchange between Fe^{2+} and Fe^{3+} causes the local displacement of charge parallel to the applied electric field. This displacement of charge results in polarization, which determines the dielectric constant and dielectric loss factors of ferrites in turn. Dielectric constant (ε') and dielectric loss factor (ε'') of all the samples were measured in the frequency (f) range of 1 kHz to 1 MHz at room temperature. Fig. 5 reveals that both the dielectric

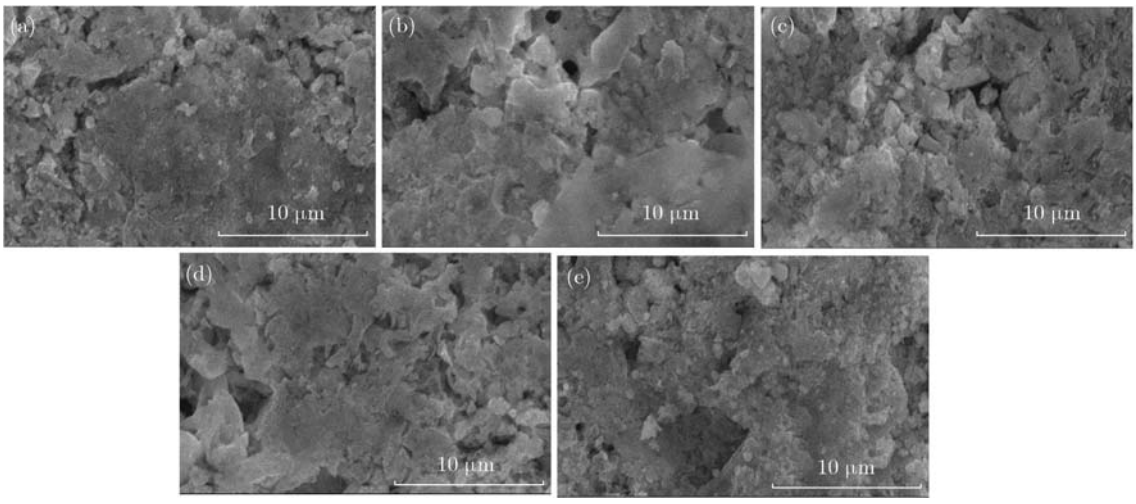

Fig. 3. SEM images of $Bi_{0.9}La_{0.1}Fe_{1-x}Co_xO_3$: (a) $x = 0$; (b) $x = 0.03$; (c) $x = 0.05$; (d) $x = 0.07$; (e) $x = 0.09$.

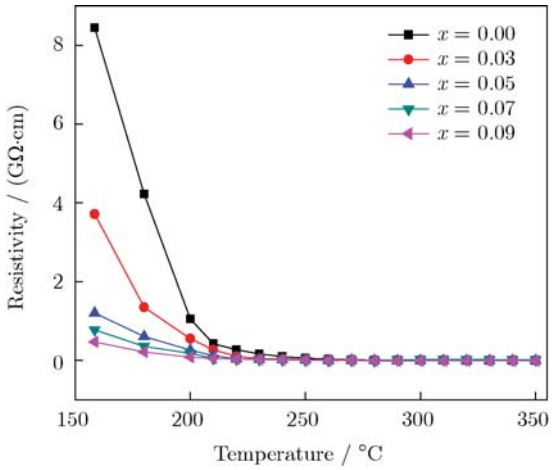

Fig. 4. Temperature-dependent resistivity of $La_{0.1}Fe_{1-x}Co_xO_3$.

constant and dielectric loss factor of all compositions decrease with the increase in frequency. The decrease in dielectric constant is related with the dielectric relaxation, which is a main cause of anomalous dispersion. In the structural view point, dielectric relaxation involves in orientation polarization, which depends on the molecular arrangement of dielectric materials [22]. Consequently, at higher frequency, the rotator motion of dielectric polar molecules is not sufficient for the attainment of equilibrium with field. Therefore, the dielectric constant appears to be constant with the increasing frequencies. In other words, at high enough frequency, the dipoles due to inertia can not align themselves in the direction in the applied field. As a result, the dielectric constant and dielectric loss factor remain almost constant [23].

3.5. Magnetic measurements

The magnetic hysteresis (M-H) loops of undoped and Co-doped samples are represented in Fig. 6. Traditionally, BFO is known to exhibit G-type antiferromagnetic characteristics [24]. However, a weak ferromagnetic behavior may be observed due to the residual magnetic moments, which is attributable to the canted spin structure [25]. This behavior is evident from the M-H loops of two samples: one without Co doping and the other with 3at% Co. In both samples, very small values of remanence (M_r) and saturation magnetization (M_s) are observed. As the Co content increases up to 9at%, gradual increases in M_r and M_s are observed, the characteristic of ferromagnetic behavior. This increased ferromagnetic characteristic of samples with the increase of Co content is well in agreement with the previously reported results and can be attributed to the breakdown of balance between the antiparallel sublattice magnetization of Fe^{3+} due to the metal ion substitution with a different valence [26].

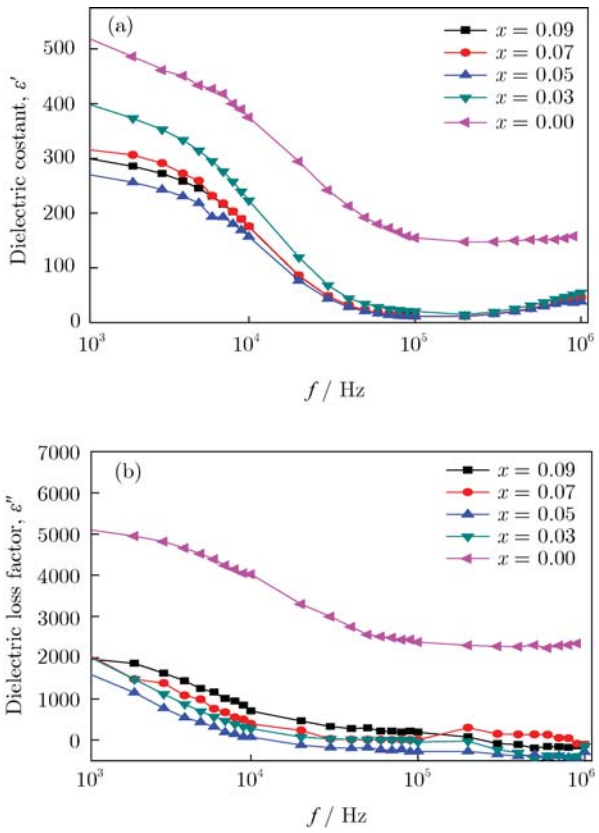

Fig. 5. Dielectric constant (a) and dielectric loss factor (b) vs. frequency.

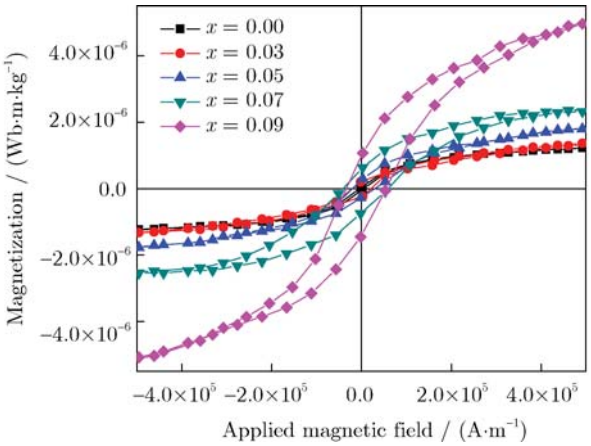

Fig. 6. Magnetic hysteresis (M-H) loops of $Bi_{0.9}La_{0.1}Fe_{1-x}Co_xO_3$.

4. Conclusions

Single-phase $Bi_{0.9}La_{0.1}FeO_3$ was successfully synthe-

sized by a sol-gel auto-combustion technique. However, a small impurity phase of $Bi_2Fe_4O_9$ was detected in all the Co-doped compositions. The lattice parameters and crystallite sizes were significantly changed with the substitution of Co at Fe sites. Morphological studies demonstrated the well-shaped bounded grains. Electrical properties of samples were investigated to find the dielectric constant and resistivity. Temperature-dependent resistivity exhibited an insulating behavior of all the samples. However, the value of electrical resistivity exhibited a decreasing trend with the increase of Co content. Ferromagnetic behavior was evident in the compositions, but the value of magnetization was enhanced with the increase in Co contents. In brief, at room temperature, the perovskite Co-doped solid solution is confirmed to display the ferromagnetic behavior.

Acknowledgements

The authors are obliged to Prof. Dr. Arshad Saleem Bhatti, Chairman, Department of Physics, Comsats Institute of Information Technology (CIIT), Islamabad, for providing the facilities of structural investigation and temperature-dependent resistivity measurements. Prof. Dr. Shahzad Naseem is also highly obliged for providing VSM and SEM facilities.

References

[1] K.F. Wang, J.M. Liu, and Z.F. Ren, Multiferroicity: the coupling between magnetic and polarization orders, *Adv. Phys.*, 58(2009), No. 4, p. 321.

[2] N. Izyumskaya, Ya. Alivov, and H. Morkoç, Oxides, oxides, and more oxides: high-κ oxides, ferroelectrics, ferromagnetics, and multiferroics, *Crit. Rev. Solid State Mater. Sci.*, 34(2009), No. 3-4, p. 89.

[3] M. Fechner, I.V. Maznichenko, S. Ostanin, A. Emst, J. Henk, P. Bruno, and I. Mertig, Magnetic phase transition in two-phase multiferroics predicted from first principles, *Phys. Rev. B*, 78(2008), No. 21, article No. 212406.

[4] S.H. Lim, M. Murakami, S.E. Lofland, A.J. Zambano, L.G.S. Riba, and I. Takeuchi, Exchange bias in thin-film $(Co/Pt)_3/Cr_2O_3$ multilayers, *J. Magn. Magn. Mater.*, 321(2009), No. 13, p. 1955.

[5] S. Shtrikman and D. Treves, Observation of the magnetoelectric effect in Cr_2O_3 powders, *Phys. Rev.*, 130(1963), No. 3, p. 986.

[6] M. Fiebig, Revival of the magnetoelectric effect, *J. Phys. D*, 38(2005), No. 8, p. R123.

[7] Y. Tokura, Multiferroics-toward strong coupling between magnetization and polarization in a solid, *J. Magn. Magn. Mater.*, 310(2007), No. 2, p. 1145.

[8] J. Wang, J.B. Neaton, V. Nagarajan, B. Liu, V. Vaithyanathan, U.V. Waghmare, H. Zheng, K.M. Rabe, M. Wuttig, R. Ramesh, S.B. Ogale, D. Viehland, D.G. Schlom, and N.A. Spaldin, Epitaxial $BiFeO_3$ multiferroic thin film heterostructures, *Science*, 299(2003), No. 5613, p. 1719.

[9] J. Wang, M.Y. Li, X.L. Liu, L. Pei, J. Liu, B.F. Yu, and X.Z. Zhao, Synthesis and multiferroic properties of $BiFeO_3$ nanotubes, *Chin. Phys. Lett.*, 26(2009), No. 11, article No. 117301.

[10] I.O. Troyanchuk, N.V. Tereshko, A.N. Chobot, M.V. Bushinsky, and K. Bärner, Weak ferromagnetism in $BiFeO_3$ doped with titanium, *Phys. B*, 404(2009), No. 21, p. 4185.

[11] L.W. Martin, S.P. Crane, Y.H. Chu, M.B. Holcomb, M. Gajek, M. Huijben, C.H. Yang, N. Balke, and R. Ramesh, Multiferroics and magnetoelectrics: thin films and nanostructures, *J. Phys. Condens. Matter*, 20(2008), No. 43, article No. 434220.

[12] J. Wei, D.S. Xue, C.F. Wu, and Z.X. Li, Enhanced ferromagnetic properties of multiferroic $Bi_{1-x}Sr_xMn_{0.2}Fe_{0.8}O_3$ synthesized by sol-gel process, *J. Alloys Compd.*, 453(2008), No. 1-2, p. 20.

[13] X.L. Yu and X.Q. An, Enhanced magnetic and optical properties of pure and (Mn, Sr) doped $BiFeO_3$ nanocrystals, *Solid State Commun.*, 149(2009), No. 17-18, p. 711.

[14] P. Singh, Y.A. Park, K.D. Sung, N. Hur, J.H. Jung, W.S. Noh, J.Y. Kim, J. Yoon, and Y. Jo, Magnetic and ferroelectric properties of epitaxial Sr-doped $BiFeO_3$ thin films, *Solid State Commun.*, 150(2010), No. 9-10, p. 431.

[15] S.R. Das, R.N. Choudhary, P. Bhattacharya, R.S. Katiyar, P. Dutta, A. Manivannan, and M.S. Seehra, Structural and multiferroic properties of La-modified $BiFeO_3$ ceramics, *J. Appl. Phys.*, 101(2007), No. 3, article No. 034104.

[16] S.T. Zhang, Y. Zhang, M.H. Lu, C.L. Du, Y.F. Chen, Z.G. Liu, Y.Y. Zhu, X.Q. Pan, and N.B. Ming, Substitution-induced phase transition and enhanced multiferroic properties of $Bi_{1-x}La_xFeO_3$ ceramics, *Appl. Phys. Lett.*, 88(2006), No. 16, article No. 162901.

[17] M. Al-Haj, X-ray diffraction and magnetization studies of $BiFeO_3$ multiferroic compounds substituted by Sm^{3+}, Gd^{3+}, Ca^{2+}, *Cryst. Res. Technol.*, 45(2010), No. 1, p. 89.

[18] D.C. Jia, J.H. Xu, W. Wang, H. Ke, and Y. Zhou, Structure and multiferroic properties of $BiFeO_3$ powders, *J. Eur. Ceram. Soc.*, 29(2009), No. 14, p. 3099.

[19] R. Mazumder and A. Sen, Effect of Pb-doping on dielectric properties of $BiFeO_3$ ceramics, *J. Alloys Compd.*, 475(2009), No. 1-2, p. 577.

[20] P. Kharel, S. Talebi, B. Ramachandran, A. Dixit, M.B. Sahana, C. Sudakar, R. Naik, M.S.R. Rao, G. Lawes, and V.M. Naik, Structural, magnetic, and electrical studies on polycrystalline transition-metal-doped $BiFeO_3$thin films, *J. Phys. Condens. Matter*, 21 (2009), No. 3, art. No. 036001.

[21] B. Zhou, Y.W. Zhang, C.S. Liao, and C.H. Yan, Magnetism

and phase transition for $CoFe_{2-x}Mn_xO_4$nanocrystalline thin films and powders, *J. Magn. Magn. Mater.*, 247(2002), No. 1, p. 70.

[22] C.P. Smyth, *Dielectric Behavior and Structure*, McGraw-Hill, New York, 1955, p. 53.

[23] I.H. Gul and A. Maqsood, Structural, magnetic and electrical properties of cobalt ferrites prepared by the sol gel route, *J. Alloys Compd.*, 465(2008), No. 1-2, p. 227.

[24] F. Azough, R. Freer, M. Thrall, R. Cernik, F. Tuna, and D. Collison, Microstructure and properties of Co-, Ni-, Zn-, Nb- and W-modified multiferroic $BiFeO_3$ ceramics, *J. Eur. Ceram. Soc.*, 30(2010), No. 3, p. 727.

[25] W.S. Kim, Y.K. Jun, K.H. Kim, and S.H. Hong, Enhanced magnetization in Co and Ta-substituted $BiFeO_3$ ceramics, *J. Magn. Magn. Mater.*, 321(2009), No. 19, p. 3262.

[26] T. Kanai, S.I. Ohkoshi, and K. Hashimoto, Magnetic, electric, and optical functionalities of $(PLZT)_x(BiFeO_3)_{1-x}$ ferroelectric-ferromagnetic thin films, *J. Phys. Chem. Solids*, 64(2003), No. 3, p. 391.